PNAS RESEARCH ARTICLE | BIOPHYSICS AND COMPUTATIONAL BIOLOGY

Cholesterol-dependent enzyme activity of human TSPO1

Weihua Qiu[a,b], Thi Kim Hoang Trinh[a,b], Claudio Catalano[a,b], Akul Mehta[a,b], Umesh R. Desai[a,b], Glen E. Kellogg[a,b], Wayne A. Hendrickson[c,d,e,1], and Youzhong Guo[a,b,1]

Affiliations are included on p. 9.

Contributed by Wayne A. Hendrickson; received December 31, 2023; accepted February 21, 2025; reviewed by Hung-Wen Liu and Robert M. Stroud

The amino acid sequence of the tryptophan-rich sensory proteins (TSPO) is substantially conserved throughout all kingdoms of life. Human mitochondrial TSPO1 (*Hs*TSPO1) binds to porphyrins and steroids, although its interactions with these molecules remains unknown. *Hs*TSPO1 is associated with numerous physiological and pathological disorders, but the underlying molecular mechanisms are unknown. Here, we disclose the finding of human mitochondrial TSPO as a cholesterol-dependent protoporphyrin IX oxygenase. The results of our biochemical characterization are consistent with structural data and evolutionary analysis. The dependence of *Hs*TSPO1 activity on cholesterol may be the result of the coevolution of this membrane protein with the membrane system. Our study provides a molecular foundation for comprehending the various roles played by mitochondrial TSPO in normal physiological and pathological situations.

TSPO | NCMN | cholesterol | protoporphyrin IX | bilindigin

Significance

The function and structure of the tryptophan-rich sensory proteins (TSPO) family have been the subject of contention. Here, we describe the finding of human mitochondrial TSPO1 as a cholesterol-dependent enzyme. This finding establishes the connections between cholesterol, protoporphyrin IX, oxygen, and TSPO1. This finding demonstrates the coevolution of TSPOs and their native lipid bilayer environment and provide a molecular basis for understanding the biochemical, cellular, physiological, and pathological roles of human TSPO1 and unify the structure and function of the TSPO family.

Tryptophan-rich sensory protein (TSPO), formerly known as peripheral benzodiazepine receptor (PBR), was identified in 1977 as one of the two major drug targets of the benzodiazepine-class drug, diazepam (Valium), alongside $GABA_A$ receptor, the central nervous system receptor (1). TSPO is also used as a biomarker for imaging by positron emission tomography (PET). PBR was renamed translocator protein in 2006 after a consensus was reached regarding its proposed function as a cholesterol transporter (2). The subsequent finding that TSPO null mice are viable and without defects in steroidogenesis (3, 4) argues against direct transporter significance, but some such role via binding partners (5) is conceivable.

Appropriately, the identification as TSPO persists. TSPO genes exist in all kingdoms of life and are highly conserved from bacteria to plants, animals, and humans. Human mitochondrial TSPO (*Hs*TSPO1) binds to porphyrins, diazepam, the PET-imaging compound PK11195, cholesterol, and its derivatives (*SI Appendix*, Fig. S1) and has been implicated in a variety of physiological and pathological conditions (6–10). *Bacillus cereus* TSPO (*Bc*TSPO) and *Xenopus tropicalis* TSPO (*Xt*TSPO) function similarly as enzymes that degrade protoporphyrin IX (PpIX) into bilindigin, a novel tetrapyrrole molecule (11). Numerous attempts have been made to determine the structure and thus elucidate the biochemical function of this mysterious membrane protein family; however, the structure and function of the TSPO family have been viewed as, at best, controversial (11–17).

Based on evolutionary principles, we proposed that *Hs*TSPO1 should also function as an enzyme. Although we have demonstrated that bacterial TSPO and frog TSPO function similarly (11), the function of *Hs*TSPO1 remains a hypothesis in the absence of direct experimental evidence. In contrast, many continue to believe that human mitochondrial TSPO functions as a cholesterol transporter despite the fact that this function has been contested (3, 4, 18–26). Due to structural uncertainties, both the *Mm*TSPO NMR structure (12) and the *Bc*TSPO crystal structure (11) have been used in subsequent research: the former as the template for structure-based drug design (27) and the latter for modeling *Hs*TSPO1 (28). The two models are irreconcilable. Resolving the controversies surrounding the structure and function of TSPO is crucial, not only for understanding the molecular mechanism of the physiological and pathological conditions in which TSPO is implicated but also for establishing a factual foundation for structure-based drug design.

In this study, we provide evidence for the dependence of *Hs*TSPO1 conformation and enzymatic activity on the presence of cholesterol. When *Hs*TSPO1 is extracted from cell membranes by a detergent, enzymatic activity is lost, and cholesterol is also lost; however, when the extraction is done with an appropriate synthetic polymer, or when detergent-extracted *Hs*TSPO1 is reconstituted an appropriate cholesterol analog, the oxidative cleavage of PpIX by *Hs*TSPO1 is then the same as that of *Bc*TSPO. The tryptophan fluorescence spectrum of *Hs*TSPO1 is also sensitive to the presence of an appropriate cholesterol analog, and its quenching by TSPO ligands depends on having *Hs*TSPO1 in the cholesterol-stabilized

Author contributions: W.Q., T.K.H.T., and Y.G. designed research; W.Q., T.K.H.T., C.C., A.M., U.R.D., G.E.K., and Y.G. performed research; Y.G. contributed new reagents/analytic tools; W.Q., W.A.H., and Y.G. analyzed data; and W.Q., W.A.H., and Y.G. wrote the paper.

Reviewers: H.-W.L., University of Texas; and R.M.S., University of California, San Francisco.

Competing interest statement: Y.G. has patents pending related to the NCMN system, PpIX-2, Billindigin and the bioactive peripheral benzodiazepine receptor. The NCMN system stands for Native Cell Membrane Nanoparticles system. It is a detergent-free system developed for membrane protein research. PpIX-2 is a derivative molecule of protoporphyrin IX that exhibits enhanced water solubility. Bilindigin is an oxidized product of protoporphyrin IX catalyzed by TSPO proteins. The bioactive peripheral benzodiazepine receptor (HsTSPO1) can be well stabilized via the NCMN system and holds potential for applications in fundamental research, pharmacological development, and other industrial uses. T.K.H.T. shares a pending patent related to PpIX-2. Y.G. and T.K.H.T co-invented CHEAPS, a cholesterol derivative molecule with a balanced hydrophobicity and hydrophilicity (marketed by Anatrace Inc., Catalog # CH240). W.Q. shares a pending patent related to the bioactive peripheral benzodiazepine receptor. Y.G. and W.Q. are the founders of a startup, NCMNtech LLC.

[1]To whom correspondence may be addressed. Email: wah2@cumc.columbia.edu or yguo4@vcu.edu.

This article contains supporting information online at https://www.pnas.org/lookup/suppl/doi:10.1073/pnas.2323045122/-/DCSupplemental.

Published March 27, 2025.

state. The crystal structure of *Bc*TSPO complexed with hemin and homology models of *Hs*TSPO1 and of its complex with PpIX support the underlying high similarity between mammalian and bacterial TSPOs, and TSPO-hemin structure provides evidence for a common tryptophan radical mechanism for the oxidative cleavage of PpIX into its bilindigin product. These findings provide compelling evidence for the commonality of TSPO structure and enzymatic function.

Results

Essentiality of the Native Lipid Environment for the Enzymatic Activity of *Hs*TSPO1. TSPO proteins share a general function as enzymes that catalyze the degradation of protoporphyrin IX into bilindigin (Fig. 1*A*). Protein instability thwarted our previous effort to fully characterize enzymatic properties for the vertebrate *Xt*TSPO, A147T *Hs*TSPO1, and *Hs*TSPO2 proteins (11). The detergent-purified *Hs*TSPO1 failed to cleave PpIX. We reasoned that over-delipidation caused by detergents might have affected the reaction, and we then sought to preserve lipid integrity by employing a polymer extraction procedure (29–33). Here, we used detergent-free native cell membrane nanoparticles (NCNM) system to maintain *Hs*TSPO1 in its native lipid environment following a modified protocol (Fig. 1*B*) (30). We also observed that *Hs*TSPO1 was more stable through purifications when fused to EGFP, but that its enzymatic activity was the same with or without the fused EGFP (*SI Appendix*, Fig. S2). Thus, we used the *Hs*TSPO1-EGFP fusion protein in our assays, which for convenience we label simply *Hs*TSPO1.

The enzyme assay is based on the photochemistry of PpIX (11, 34). Briefly, PpIX excitation by blue-violet light of around 405 nm produces fluorescence with a prominent peak at approximately 635 nm, and TSPO-catalyzed oxygenation of PpIX is accompanied by the decay of this fluorescence consequent to cleavage of PpIX into bilindigin (11). Photostimulation of PpIX generates singlet oxygen and other reactive oxygen species (ROS) (35, 36), and we suggest that cellular ROS acting with tryptophan radicals at W51 and W138 (*Bc*TSPO numbering) degrades PpIX for ROS neutralization (11). PpIX is a highly hydrophobic molecule, but it was solubilized adventitiously when added to detergent-solubilized TSPO. Our NCMN system is detergent-free to avoid over-delipidation that might perturb the enzymatic activity. Thus, the assay needed to be adapted for NCMN-encapsulated TSPO.

To overcome the assay complication, we designed and synthesized a PpIX derivative termed PpIX-2 (*SI Appendix*, Fig. S3). PpIX-2 retains the core porphyrin structure of protoporphyrin IX, but it has much-increased water solubility, making it compatible with the detergent-free NCMN system. We confirmed that PpIX-2 has precisely the same photochemical properties as those of PpIX. When NCMN-solubilized *Hs*TSPO1 is light-activated, it degrades PpIX-2 irreversibly and produces spectra (Fig. 1 *C* and *D*) that are qualitatively the same as those from DDM-solubilized

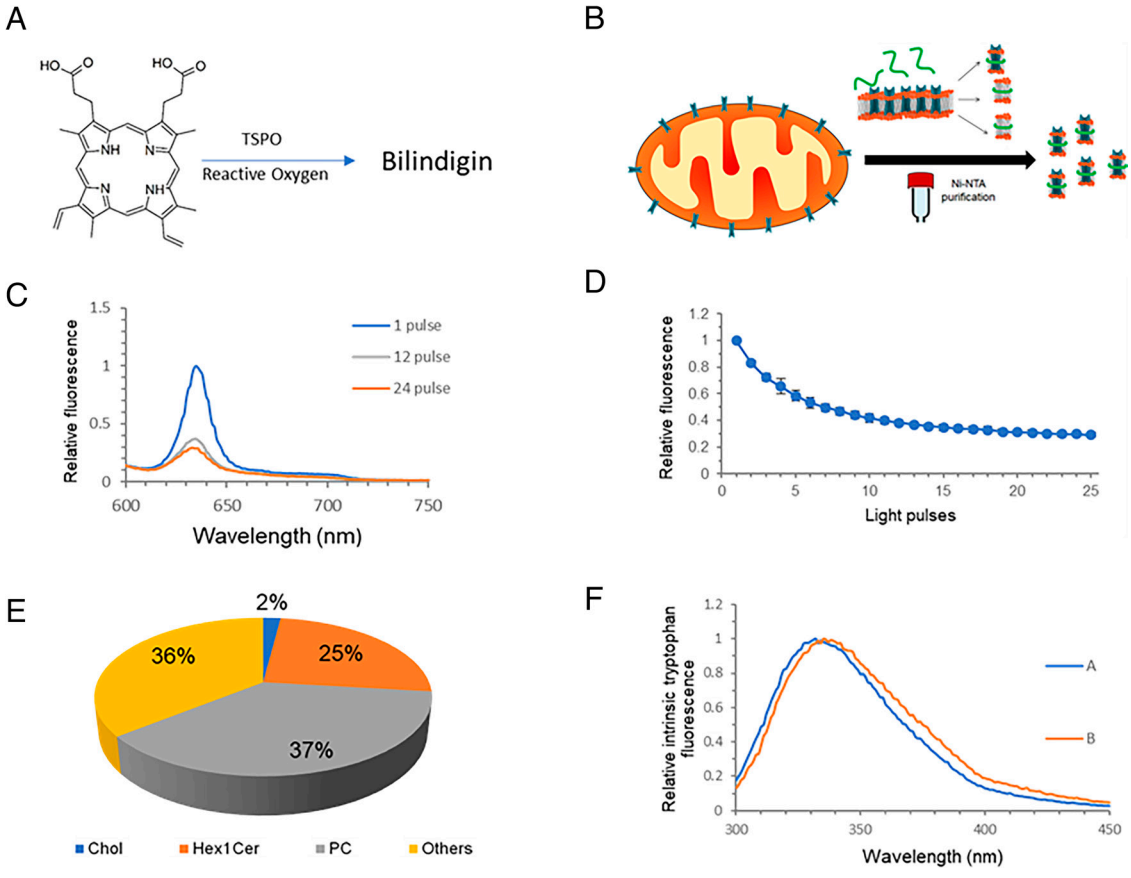

Fig. 1. Enzyme activity and lipid dependency of *Hs*TSPO1. (*A*) The general enzymatic reaction catalyzed by TSPO protein. TSPO catalyze the oxidative degradation of protoporphyrin IX into bilindigin. (*B*). The diagram shows the general procedure for preparation of *Hs*TSPO1 NCMN particles. *Hs*TSPO1 is a conserved mitochondrial membrane protein. Membrane-active polymers can extract *Hs*TSPO1 directly from the mitochondrial membrane. After a single-step affinity purification, *Hs*TSPO1 NCMN particles can be produced in the active state with associated native cell membrane lipids. (*C*). Fluorescence spectra showing *Hs*TSPO1 enzyme activity. The enzyme activity was monitored by fluorescence decay of protoporphyrin IX-2 at 632 nm upon excitation at 405 nm with different doses of light pulses. (*D*) The light-pulse-dose-dependent fluorescence decay of protoporphyrin IX-2 upon exposure to UV 405 nm. (*E*) Lipidomic analysis of *Hs*TSPO1 NCMN particles showing relative amount of different native lipid species that associated with *Hs*TSPO1. Chol: cholesterol, Hex1Cer: Hex1 ceramide, PC: phosphatidylcholines. (*F*) Comparison of intrinsic tryptophan fluorescence spectrum *Hs*TSPO1 in the presence of CHS ($_A$) and inactive *Hs*TSPO1 in the absence of CHS ($_B$).

*Bc*TSPO (11). In contrast, with either DDM-solubilized *Bc*TSPO or with freshly DDM-solubilized *Hs*TSPO1 in the absence of CHS showed a PpIX excited-state fluorescence excitation that emerges at 673 nm as the 632-nm peak decreases (Fig. 2*A*). These results imply that the lipid membrane environment is crucial for the functionality of *Hs*TSPO1.

We next used lipidomic analysis by mass spectrometry to identify natively associated lipids in mitochondrial membranes and in NCMN-extracted TSPO particles (Fig. 1*E*). It has been debated whether *Hs*TSPO1 is a cholesterol transporter; however, it is consensual that *Hs*TSPO1 binds to cholesterol (37, 38). Indeed, cholesterol is retained with TSPO in the NCMN particles (Fig. 1*E*), whereas *Hs*TSPO1 is over-delipidated during extraction with detergents, such as DDM and LMNG. When *Hs*TSPO1 is stabilized with CHS, a genuine cholesterol analog, its tryptophan fluorescence spectrum implies a distinctive conformation (Fig. 1*F*) and its enzyme activity (Fig. 2*A*) is indistinguishable from that of *Bc*TSPO.

Cholesterol Dependence of *Hs*TSPO1 Enzymatic Activity. Which of the lipid components is the crucial one? Cholesterol has long been implicated in *Hs*TSPO1 activity and cholesterol is a distinguishing characteristic of animals compared to bacterial membranes. Thus, given the distinctions between *Hs*TSPO1 photochemistry and that of *Bc*TSPO, we reasoned that cholesterol might be critical for enzymatic activity instead of being transported by TSPO (2). To test this hypothesis, we returned to detergent-solubilized *Hs*TSPO1, which is stripped of lipids. We then purified the *Hs*TSPO1 with and without high concentrations of the soluble cholesterol analog cholesteryl hemisuccinate (CHS). We found that *Hs*TSPO1 displayed distinct intrinsic tryptophan fluorescence spectra in the presence of CHS as compared with its absence; the absence of CHS led to 6 nm red shift (*Hs*TSPO1/CHS gave a fluorescence peak at 332 nm; *Hs*TSPO1 gave a fluorescence peak at 338 nm) (Fig. 1*F*).

We found that the photochemical properties of DDM-extracted *Hs*TSPO1 toward the PpIX substrate in the absence of CHS (Fig. 2*A*) are similar to those of the *Hs*TSPO1 A147T and *Bc*TSPO A142T mutants, which can bind to PpIX but has lost catalytic activity. The photochemical properties of DDM-extracted *Hs*TSPO1 toward PpIX in the presence of CHS (Fig. 2*B*) are essentially identical to those toward the PpIX-2 substrate by NCMN-extracted *Hs*TSPO1 (Fig. 1 *C* and *D*) and of DDM-extracted wild-type (WT) *Bc*TSPO, which has the catalytic activity. Furthermore, this PpIX fluorescence spectral progression for

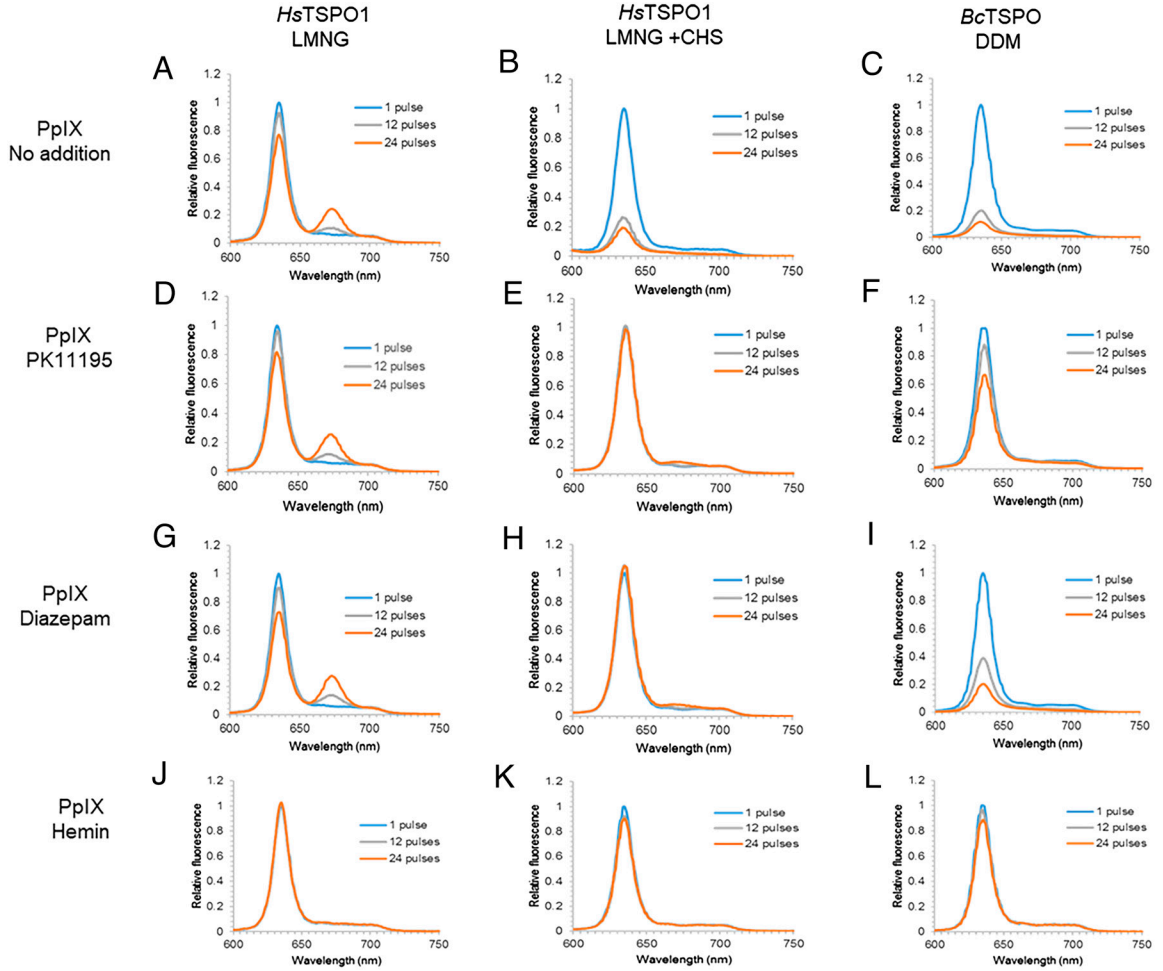

Fig. 2. Comparative characterization of enzyme activities of *Hs*TSPO1 and *Bc*TSPO. Photoactivated fluorescence spectra are shown for various TSPO-PpIX preparations. (*A–C*) show the enzyme activity of *Hs*TSPO1 and *Bc*TSPO without additional inhibitors. (*D–F*) show the enzyme activity of HsTSPO1 and *Bc*TSPO with PK11195 as inhibitors. (*G–I*) show the enzyme activity of *Hs*TSPO1 and *Bc*TSPO with diazepam as an inhibitor. (*J–L*) show the enzyme activity of *Hs*TSPO1 and *Bc*TSPO with hemin as an inhibitor. (*A*, *D*, *G*, and *J*) show DDM and LMNG-purified *Hs*TSPO1 without CHS. (*B*, *E*, *H*, and *K*) show DDM and LMNG-purified *Hs*TSPO1 with CHS. (*C*, *F*, *I*, and *L*) show *Bc*TSPO purified without CHS. (*J*, *K*, and *L*) show the enzyme activity of HsTSPO1 and BcTSPO with hemin as an inhibitor. (*A*) shows that, in the absence of CHS, *Hs*TSPO1 binds to PpIX but does not degrade PpIX into bilindigin as indicated by the decrease of peak 632 nm and appearance of the peak of 673 nm. (*B* and *C*) show that *Hs*TSPO1 in the presence of CHS has similar enzyme activity as that of *Bc*TSPO; (*E*, *H*, *K* and *F*, *I*, *L*) show that PK11195, Diazepam and Hemin inhibit both *Hs*TSPO1 and *Bc*TSPO; (*D* and *G*) show in the absence of CHS, PK11195, and Diazepam do not have obvious inhibition of PpIX binding to *Hs*TSPO1; (*J*) shows that even in the absence of CHS, hemin inhibit binding of PpIX to *Hs*TSPO1.

*Hs*TSPO1 in the presence of CHS is very similar to that for *Bc*TSPO, indicating that the human and bacterial TSPOs have very similar enzymatic activities provided that *Hs*TSPO1 is in an appropriate cholesterol environment (Fig. 2 *B* and *C*).

We also tried CHAPS and CHAPSO detergents, which are alternative cholesterol analogs. Neither of these could preserve the enzyme activity of *Hs*TSPO1; the fluorescence spectra of PpIX are unchanged with light exposure (*SI Appendix*, Fig. S4 *A–D*, respectively). This situation is similar to the Fos-choline-treated *Hs*TSPO1 sample (*SI Appendix*, Fig. S4 *E* and *F*). By contrast, an alternative analog, CHEAPS, elicits enzymatic activity similar to CHS. We designed and synthesized CHEAPS for better solubility than CHS in detergent and compatibility with our NCMN library (39). Both CHS and CHEAPS derivatize cholesterol at the 3-β hydroxyl group (*SI Appendix*, Fig. S1 *E* and *I*). In contrast, CHAPSO and CHAPS replace the hydrophobic carbon tail at C17 of the four-ring steroid nucleus (*SI Appendix*, Fig. S1 *G* and *H*). It appears that both the aliphatic tail of cholesterol and the four-ring steroid nucleus are essential for proper activity (*SI Appendix*, Fig. S1*F*).

Shared Inhibition Characteristics of Human and Bacterial TSPO Enzymatic Activities. We show above that *Hs*TSPO1 and *Bc*TSPO degrade PpIX with similar kinetics, provided that the human protein is cholesterol-associated. We show here that both enzymes are also similarly inhibited by relevant compounds. The PET-imaging agent PK11195 was designed to bind to *Hs*TSPO1, but we showed that it also binds to *Bc*TSPO and partially inhibits its enzymatic activity. Diazepam is the PBR namesake for what is now known as TSPO, and its binding to *Hs*TSPO1 is comparable with that of PK11195. We previously proposed that PpIX binds to the same highly conserved cavity in *Bc*TSPO at which PK11195 binds. Chlorohemin is the chloride salt of Fe(III)-PpIX, and chlorohemin can spontaneously convert to hematin in an alkaline solution (40); as reduced to Fe(II)-PpIX, it is known as heme. We surmised that Fe-PpIX might bind to TSPOs in a manner analogous to that of the PpIX substrate and tested its effects on the reaction.

The photochemical reaction of *Hs*TSPO1 in CHS with PpIX is almost completely inhibited by PK11195, diazepam, or Fe-PpIX (Fig. 2 *E*, *H*, and *K*). Similarly, the reaction of *Bc*TSPO1 with PpIX is mostly inhibited by PK11195 and completely so by Fe-PpIX, but diazepam has much less effect (Fig. 2 *F*, *I*, and *L*). When *Hs*TSPO1 is reacted without CHS being present, neither PK11195 nor diazepam has a measurable effect (Fig. 2 *D* and *G*); however, Fe-PpIX inhibits *Hs*TSPO1 photochemistry completely even in the absence of the cholesterol analog (Fig. 2 *J* and *K*).

We interpret these results on the effects of PK11195, diazepam, and Fe-PpIX on TSPO enzymatic activities, confirming the essential similarity of human and bacterial TSPOs as enzymes. All three compounds block PpIX degradation completely, presumably because they bind tightly to *Hs*TSPO1. Fe-PpIX, a direct analog of the actual substrate, is also an effective inhibitor of all three TSPO preparations. The variability in response to the other two reagents likely reflects the relative affinity of each reagent to the two TSPOs. PK11195 binds quite well to *Bc*TSPO as it does to *Hs*TSPO1, and it blocks the reaction appreciably (Fig. 2 *E* and *F*), whereas diazepam shows only limited blockage of *Bc*TSPO activity (Fig. 2*I*). As shown before (Fig. 1*F*), the conformation of *Hs*TSPO1 in the absence of an authentic cholesterol analog differs markedly from that in CHS; it appears that this cholesterol-free state has little affinity for PK11195 or diazepam but that an induced fit to Fe-PpIX is facile. Taken altogether, both TSPO proteins degrade PpIX in a similar manner.

Sensitivity of *Hs*TSPO1 Conformation to Cholesterol and Environmental Conditions. The striking distinctions between the photochemical reactions of PpIX with *Hs*TSPO1 when in the presence and absence of cholesterol suggest that the protein conformation must differ for the two situations. Intrinsic tryptophan fluorescence is sensitive to the indole surroundings, becoming red-shifted when in a less hydrophobic environment (41). Being "tryptophan rich" as stated in the namesake *Rs*TSPO, sensitivity of TSPO intrinsic fluorescence to conformation can be expected, but the very richness (12 tryptophan among the 169 residues in *Hs*TSPO1) complicates interpretation. Conformational change in the protein perturbs each tryptophan environment and its fluorescence differently, but only the averaged spectral output is measured.

When *Hs*TSPO1 is in its enzymatically active state, as associated with a genuine cholesterol analog such as CHS, the tryptophan fluorescence maximum is at 332 nm (Fig. 1*F*); however, the spectrum from *Hs*TSPO1 in the absence of a cholesterol analog is red-shifted to a maximum at 338 nm (Fig. 1*F*). This shift of 6 nm is substantial, especially considering the numerous tryptophan residues; for comparison, Hsp70 DnaK, a single-tryptophan protein, blue shifts by 7 nm when ATP replaces ADP (42), which entails a hydrophobic covering of the indole ring when an interdomain interface forms in the ATP-bound restraining state (43).

Quite generally, a blue-shifted intrinsic fluorescence spectrum (332 nm maximum) corresponds with enzymatic activity; wherein, as for WT *Bc*TSPO, the photoactivated PpIX emission at 632 nm disappears as *Hs*TSPO1 degrades PpIX with increasing illumination (Fig. 1 *C* and *D*, NCNM-extracted; Fig. 2*B*, CHS-stabilized). The red-shifted alternative (338 nm maximum) does not support PpIX degradation; instead, the photochemistry generates persistent excited-state emission at 673 nm and abated loss of 632 nm emission with illumination (Figs. 2 *A*, *D*, and *G*, detergent-extracted without CHS), similarly as for the enzymatically inert W51F/W138F mutant of *Bc*TSPO (11). Conditions wherein *Hs*TSPO1 binds PpIX without spectral change on light exposure (e.g., 1% CHAPS or CHAPSO, *SI Appendix*, Fig. S4 *A–D*) or that are denaturing with no PpIX interaction (e.g., 6 M urea) also yield tryptophan fluorescence spectra with maxima at ~338 nm (Fig. 3 *A–C*). In the case of CHAPS in the presence of CHS (Fig. 3*C*), the spectrum depends on the relative concentrations; at a high ratio of CHAPS to CHS, CHAPS displaces CHS, whereupon the spectrum simply reverts to that of CHS-free *Hs*TSPO1. Thus, the cholesterol-associated active state of *Hs*TSPO1 has a distinctive conformation, one with greater hydrophobic contacts to the indole groups than when without cholesterol.

Since the NMR structure of *Mm*TSPO was determined in dodecyl phosphocholine (DPC) micelles, we also measured the intrinsic tryptophan fluorescence of *Hs*TSPO1 in 2% DPC (Fig. 3*C*). This spectrum is also red-shifted and most similar to that for *Hs*TSPO1 in 6 M urea (Fig. 3*A*). When heated to 40 °C in 2% DPC, as used for the NMR analysis of *Mm*TSPO, the *Hs*TSPO1 fluorescence spectrum is shifted still further to longer wavelengths (Fig. 3*C*). The effect of DPC on the photoactivity of PpIX was also tested in the presence of 2% DPC, and we found no change in PpIX fluorescence on light exposure (*SI Appendix*, Fig. S4 *E* and *F*). DPC is a relatively harsh detergent, and we conclude that the conformation of *Hs*TSPO1 in DPC is not biologically relevant, a conclusion also supported by a comprehensive analysis of DPC effects on membrane protein structure (44).

Quenching of Tryptophan Fluorescence Upon Orthosteric Ligand Binding to *Hs*TSPO1. We previously showed that both diazepam and PK11195 bind into a tryptophan-lined pocket of *Bc*TSPO,

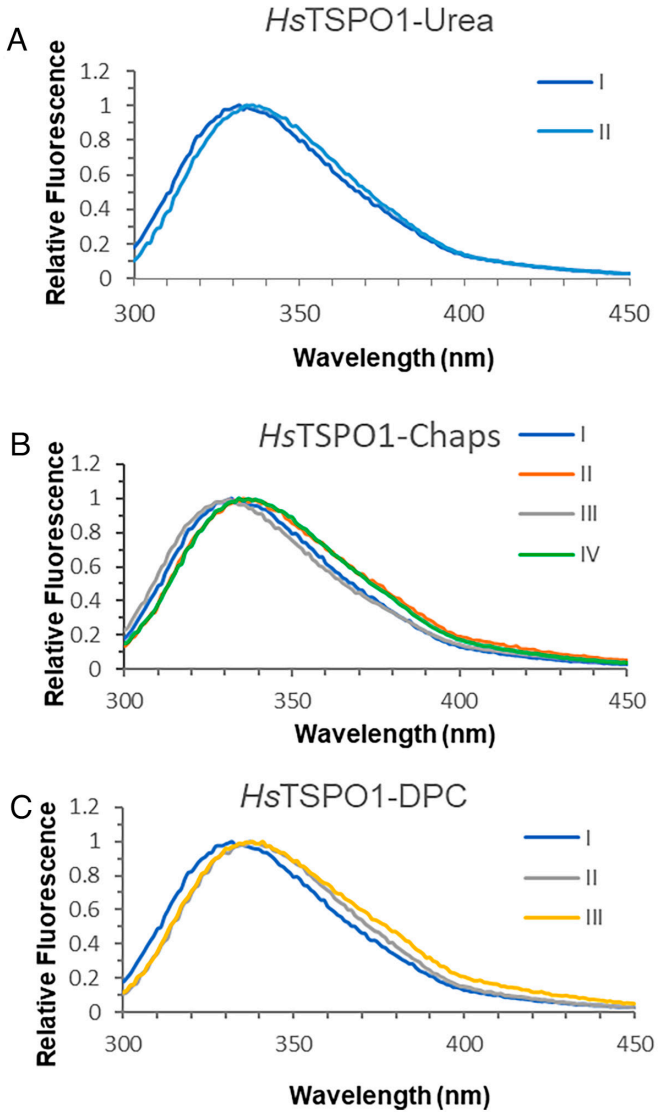

Fig. 3. Red-shifting impact of urea, CHAPS, and DPC on the intrinsic *Hs*TSPO1 tryptophan fluorescence in the presence of CHS. (*A*) I, Control, active *Hs*TSPO1 in the presence of 0.02% CHS and 0.05%v LMNG; II, *Hs*TSPO1 in the presence of 0.02% CHS and 0.05%v LMNG and 6 M of Urea; (*B*) I, Control, active *Hs*TSPO1 in the presence of 0.02% CHS, 0.05%v LMNG, and 0% CHAPS; II, *Hs*TSPO1 in the presence of 0.02% CHS and 0.05%v LMNG and 1% CHAPS; III, *Hs*TSPO1 in the presence of 0.02% CHS and 0.05%v LMNG and 0.02% CHAPS; IV, *Hs*TSPO1 in the presence of 0.05%v LMNG and absence of CHS; (*C*) I, Control, active *Hs*TSPO1 in the presence of 0.02% CHS and 0.05%v LMNG; II, *Hs*TSPO1 in the presence of 0.02% CHS and 0.05%v LMNG and 2% DPC without heating; III, *Hs*TSPO1 in the presence of 0.02% CHS and 0.05%v LMNG and 2% DPC and heated at 40 °C for 30 min.

and a model for the binding of PpIX into this same pocket is now validated by the structures of *Bc*TSPO (vida infra) and *Rs*TSPO (45) as bound to heme. Hence, diazepam and PK11195 are orthosteric to the physiological PpIX substrate. This pocket remains tryptophan-rich in our homology model of *Hs*TSPO1. Strong quenching of tryptophan fluorescence has been observed when PpIX and other ligands bind to bacterial TSPOs (46, 47), here, we examine the quenching of tryptophan fluorescence in *Hs*TSPO1 by PpIX and orthosteric ligands as affected by the cholesterol analog CHS.

All of these ligands quench the intrinsic tryptophan fluorescence of *Hs*TPSO1, but with varying dependence on the presence of CHS. Hemin quenches very strongly whether CHS is present or not (Fig. 4 *A* and *B*), PpIX is somewhat less potent in quenching and its effectiveness is attenuated in the absence of CHS (Fig. 4 *C* and *D*), and both diazepam and PK11195 are quenchers in the presence of CHS but hardly at all in its absence (Fig. 4 *E*–*H* and *SI Appendix*, Fig. S5 presents the complete set of quenching experiments from which Fig. 4 is extracted. These findings correlate with the potency of inhibition of enzymatic activity against PpIX by these ligands (Fig. 2), and they are in accord with a conformational equilibrium that favors an inactive, nonbinding state without cholesterol being present and with binding propensities in the order hemin > PpIX > PK11195 ≈ diazepam. Intrinsic quenching potencies of the ligands also vary, with the saturation of quenching for PK11195 and diazepam independent of concentration.

It has been suggested that cholesterol may bind into the same ligand pocket (46, 47); however, we found no quenching of *Hs*TPSO1 by CHS (*SI Appendix*, Fig. S5*I*). It is possible that the solubilizing moiety attached to the 3-β hydroxyl group would block entry into the pocket; however, we also find no quenching by CHAPS (*SI Appendix*, Fig. S5*J*), for which the solubilizing moiety replaces the hydrophobic carbon tail at C17 at the opposite end of the four-ring core. We suggest that cholesterol binds to *Hs*TPSO1 at an external surface and in contact with the lipid bilayer. The insolubility of cholesterol has thwarted our attempts to test it directly, although consequent clouding gave the impression of profound attenuation of tryptophan fluorescence.

Structure of the Protoporphyrin IX Complex with TSPO and Enzymatic Consequences. As shown above (Fig. 2 *J*–*L*), Fe-PpIX inhibits the enzymatic activity of both *Hs*TSPO1 and *Bc*TSPO toward PpIX. We had shown previously that PpIX can be fitted into the highly conserved cavity in the *Bc*TSPO structure (11). Here, we confirm that modeling with a crystal structure of the complex with the Fe-PpIX (hematin) inhibitor at 2.0 Å resolution (Fig. 5 *A* and *B*). The porphyrin moiety binds with its vinyl-substituted rings deep into the ligand pocket and its propionate groups facing the aqueous environment. The *Bc*TSPO protein itself has essentially the same structure in the complex as in the apo state, except that the $\alpha_{1,2}$-containing loop between TM1 and TM2 moves appreciably to a placement superimposable with that in our previously described structure of the PK11195–*Bc*TSPO complex (*SI Appendix*, Fig. S6 *A* and *B*). In keeping with the high degree of conservation in pocket-lining TSPO residues (Fig. 5 *C*–*E*), five of the ten residues in vdW contact with the porphyrin moiety are identical to their *Bc*TSPO counterparts; three others are chemically equivalent (I→F, F→Y, F→W), and all are fully accommodated in a homology model of *Hs*TSPO1 (*SI Appendix*, Figs. S7 and S8).

The molecular basis for cholesterol stabilization of *Hs*TSPO1 is unclear, but an important clue is provided from the characteristics of sequence conservation. As noted above, the ligand-binding pocket is highly conserved, and this conservation is clear when viewed into the pocket between helices TM1 and TM2 (Fig. 5 *A*, *C*, and *E*). A second region of high conservation is also evident at the bilayer-contacting surface between TM2 and TM5 (Fig. 5 *B* and *D*), and we suggest that this might be the site taken by a conformation-stabilizing cholesterol molecule (*SI Appendix*, Figs. S9 and S10). This site includes the LAF sequence between W138 and A142 of *Hs*TSPO1, which confers markedly enhanced cholesterol binding to *Rs*TSPO when this human sequence is substituted in place of the corresponding ATA WT *R. spheroides* sequence (48).

The quasi-diad symmetric Fe-PpIX is unambiguously and stereo-specifically located in the ligand pockets of both copies in the asymmetric unit (*SI Appendix*, Fig. S5*C*). Methine-bridging carbon atom α, between the vinyl-bearing pyrrolidine rings

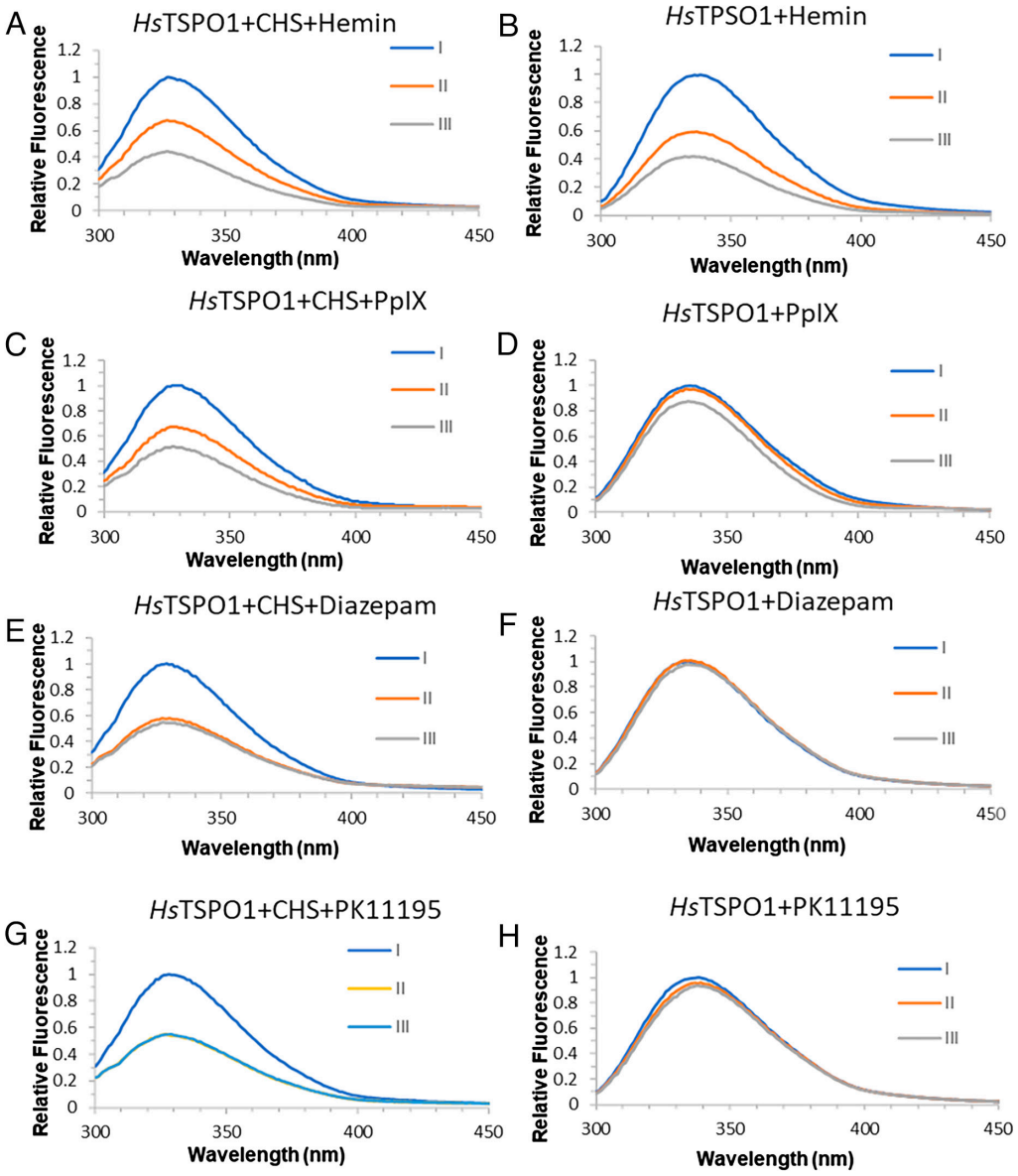

Fig. 4. Intrinsic tryptophan fluorescence analysis of *Hs*TSPO1 in the presence and absence of CHS. (*A*) Intrinsic tryptophan fluorescence quenching spectra of *Hs*TSPO1 in the presence of 0.02% CHS and various concentrations of hemin. I, 0 μL of 1 mg/mL hemin; II, 1μL of 1 mg/mL hemin; III, 2 μL of 1 mg/mL hemin; (*B*) Intrinsic tryptophan fluorescence quenching spectra of *Hs*TSPO1 in the absence of CHS and various concentrations of hemin. I, 0μL of 1 mg/mL hemin; II, 1μL of 1 mg/mL hemin; III, 2 μL of 1 mg/mL hemin; (*C*) Intrinsic tryptophan fluorescence quenching spectra of *Hs*TSPO1 in the presence of 0.02% CHS and various concentrations of PpIX. I, 0μL of 1 mg/mL PpIX; II, 1 μL of 1 mg/mL PpIX; III, 2 μL of 1 mg/mL PpIX; (*D*) Intrinsic tryptophan fluorescence quenching spectra of *Hs*TSPO1 in the absence of 0.02% CHS and various concentrations of PpIX. I, 0 μL of 1 mg/mL PpIX; II, 1 μL of 1 mg/mL PpIX; III, 2 μL of 1 mg/mL PpIX; (*E*) Intrinsic tryptophan fluorescence quenching spectra of *Hs*TSPO1 in the presence of 0.02% CHS and various concentrations of diazepam. I, 0 μL of 1 mg/mL Diazepam; II, 1 μ L of 1 mg/mL Diazepam; III, 2 μ L of 1 mg/mL Diazepam; (*F*) Intrinsic tryptophan fluorescence quenching spectra of *Hs*TSPO1 in the absence of CHS and various concentrations of diazepam. I, 0 μL of 1 mg/mL PK11195; II, 1 μL of 1 mg/mL PK11195; III, 2 μL of 1 mg/mL PK11195; (*G*) Intrinsic tryptophan fluorescence quenching spectra of *Hs*TSPO1 in the presence of 0.02% CHS and various concentrations of PK11195. I, 0 μL of 1 mg/mL PK11195; II, 1 μ L of 1 mg/mL PK11195; III, 2 μ L of 1 mg/mL PK11195; (*H*) Intrinsic tryptophan fluorescence quenching spectra of *Hs*TSPO1 in the absence of CHS and various concentrations of PK11195. I, 0 μL of 1 mg/mL PK11195; II, 1 μL of 1 mg/mL PK11195; III, 2 μL of 1 mg/mL PK11195.

(A and B), is close to the indole nitrogen atoms of conserved tryptophan residues W51 and W138 (Fig. 5*F*), which are implicated by mutational analysis in the enzymatic oxidation reaction (11). We speculate that the reaction mechanism involves the participation of tryptophan radicals, which can be activated either by photochemistry, as in our experiments here, or by cell ROS. Conserved W31 and W40 have their indole nitrogen atoms placed equivalently distant (11 to 12 Å) from the vinyl group from ring A and more distant from the α methine bridge (Fig. 5*F*); however, we do not otherwise understand the basis for their conservation.

Heme oxygenase cleaves heme at methine carbon α to yield biliverdin, and the proximity of this atom to the hypothetical radical site on enzymatically critical W51 suggests that TSPO also acts at this site to produce the spectroscopically related product bilindigin (11). The chemical structure of bilindigin is not fully known; however, we have used liquid chromatography–mass spectral analysis (UPLC–MS) to identify the masses (595 Da) and limit possible chemical structures for bilindigin and related PpIX derivatives (Fig. 5*G* and *SI Appendix*, Figs. S11 and S12). A few options are conceivable to account for the mass of bilindigin, which is precisely two oxygen atoms heavier than PpIX. Parsimoniously, a methine carbon atom could be replaced by a carbonyl group on one side and a formyl group on the other, and most plausibly here, this would have happened at methine α.

Ferguson-Miller and colleagues (45) recently described heme complexes with *Rs*TSPO mutant variants A138F and A139T

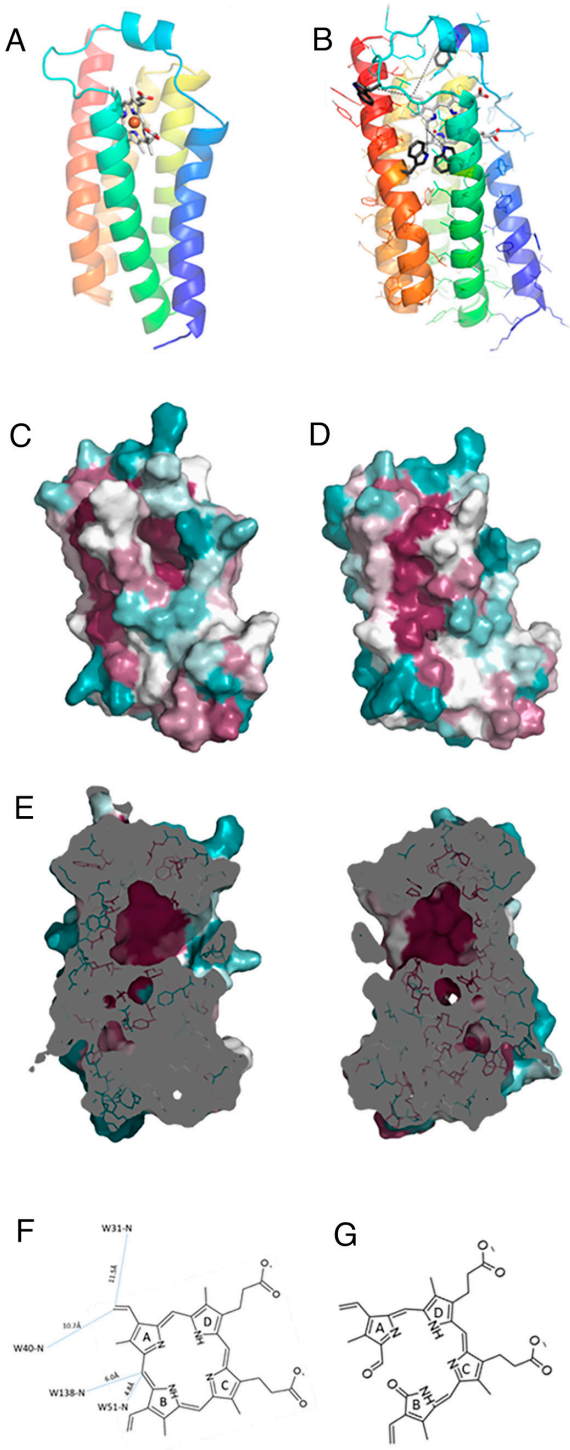

Fig. 5. Crystal structure of the *Bc*TSPO/hematin complex (PDB ID: 8VGU, chain (*A*) A single hemin molecule is located in the active site of *Bc*TSPO. (*B*) Interaction between hemin and *Bc*TSPO and relative positions of the four conserved tryptophan residues to the porphyrin molecule. (*C*) Conservativeness of the active site and potential cholesterol binding site on the *Hs*TSPO1 structural model. (*D*) Conserved potential cholesterol binding site between TM2 and TM5 on the surface of the *Hs*TSPO1 structural model. 60° anticlockwise rotation (viewed from *Top* to *Bottom*) relative to the orientation displayed in panel (*D* and *E*) Conservativeness of the active site of *Hs*TSPO1 structural model. The active site is displayed as an open-book view, i.e., 180° relative to each half of the active site. (*F*) 2D view of the relative positions of conserved tryptophan's and hemin. (*G*) 2D chemical structure of proposed bilindigin molecule based on mass spectrometric analysis.

*Rs*TSPO. The *Rs*TSPO and *Bc*TSPO structures themselves are very similar to one another (11), and the heme group is associated very similarly in the two cases, and this association is also very similar to that in our model of PpIX with *Bc*TSPO (11). Interestingly, the structures of Fe-PpIX prove to include molecular oxygen coordinated at one side of the heme plane and a water molecule at the other; however, these additions are on opposite sides in the two TSPO molecules in the asymmetric unit of the crystal (*SI Appendix*, Fig. S6*C*). Molecular oxygen is the most likely source for the TSPO-catalyzed oxygenation reaction; however, apart from demonstrating the availability of space, the oxygen and water molecules associated with Fe-PpIX here would not relate to those in TSPO-mediated catalysis.

Discussion

We compared the enzyme activities of *Hs*TSPO1 and *Bc*TSPO in the presence or absence of inhibitors, cholesterol or its analog, CHS, and DPC (Fos-choline) detergent. We established that *Hs*TSPO1 is a genuine enzyme, but one dependent on cholesterol for its activity. The crystal structure of a *Bc*TSPO/hematin complex at 2.0-Å resolution and structural modeling of *Hs*TSPO1 revealed a highly conserved active site within *Hs*TSPO1 and provided a structural basis for understanding this enzyme's activity. The recently reported crystal structures of *Rs*TSPO/heme complexes also show a similar binding mode of porphyrin to the common enzyme active site of TSPO (45). The structural analysis is consistent with biochemical characterization.

We have established *Hs*TSPO1 as an enzyme similar to *Bc*TSPO with a sequence identity of 26.6% (11); however, the *Hs*TSPO1 enzyme activity is strictly cholesterol-dependent. This dependence may result from the coevolution of TSPO proteins and their lipid membrane surroundings. Our findings contribute to resolving controversies regarding the structure and function of *Hs*TSPO1. How cholesterol binds to *Hs*TSPO1 to stabilize it for enzymatic activity will not be known in detail until a high-resolution structural determination of the *Hs*TSPO1/cholesterol complex is completed, which is currently ongoing in our laboratory. However, based on modeling of the conserved surface of *Hs*TSPO1, docking, and molecular dynamic analysis, we are able to propose a rough structural model of the *Hs*TSPO1/cholesterol complex (*SI Appendix*, Figs. S9 and S10)

Why the protein stability and enzyme activity of *Hs*TSPO1 should be cholesterol-dependent, whereas *Bc*TSPO is intrinsically stable and enzymatically active is unclear; however, a plausible explanation comes from the coevolution of TSPO with its membrane environment. The mitochondria of eukaryotes are thought to have evolved from endosymbiotic purple α-proteobacteria (49), whereas bacteria do not produce cholesterol, metazoan animals do so. Thereby, mitochondrial membranes have acquired cholesterol (albeit at lower levels than in plasma membranes). As eukaryotic TSPOs evolved in this lipid milieu, potentially destabilizing but otherwise neutral mutations could be compensated by cholesterol from the membrane. When detergent-extracted from eukaryotic membranes, membrane proteins are commonly less stable than those from bacteria unless associated with specific lipids (50).

The finding of the biochemical function of *Hs*TSPO1 as an enzyme is only the beginning of TSPO's physiological roles in numerous pathological and physiological conditions. Because cholesterol contributes to the structural integrity of *Hs*TSPO1 and does not compete for the PpIX binding pocket, the likelihood of TSPO functioning as a cholesterol transporter is minimal. In the in vitro enzyme reaction, photosensitive protoporphyrin IX, light, and oxygen are required; however, in mitochondria, the reaction is most likely mediated by singlet oxygen and other free radicals. Therefore, in order to comprehend the cellular and physiological function, we propose that future research in the field of

mitochondrial TSPO should concentrate on the porphyrin metabolism and ROS regulation and not on the cholesterol or steroid hormone metabolism.

The development of PET imaging probe molecules that target TSPO is the focus of a substantial amount of current research (51–55). However, the structural controversies described previously have made it unclear which structural model should be employed when designing such agents. The results and analyses presented here are intended to accelerate the development of PET imaging probes. The TSPO family of proteins is highly conserved, and their enzyme functions are remarkably similar. Therefore, it is reasonable to assume that the TSPO proteins of all living organisms share a similar structure. Our finding of the cholesterol-dependent enzyme activity of *Hs*TSPO1 illustrates the fact that lipids are essential to the integrity of membrane protein structure and function. We hypothesize that *Hs*TSPO1 may serve as a sensor for the oxidative state of cells, thereby eliciting an adaptive cellular response.

Contact for Reagent and Resource Sharing. Further information and requests for resources and reagents should be directed to and will be fulfilled by the Lead Contact Youzhong Guo (yguo4@vcu.edu).

Materials and Methods

***Bc*TSPO Expression and Purification.** N-terminally 10×His-tagged *Bc*TSPO in the pMCSG7 expression vector was transformed into *E. coli* BL21 (DE3) *pLysS* strain. For the structural and activity study, *Bc*TSPO expression and purification were performed per the previous protocol (11).

***Bc*TSPO/hematin Complex Crystallization.** Hemin has a dark black color when it is dissolved in DMSO. Once this solution was mixed with a protein solution (pH 7.8), the black color changed into brown or brownish/reddish, as indicated by the brown-colored crystals (*SI Appendix*, Fig. S13). In this aqueous alkali condition, hemin spontaneously converts into hematin and replaces Cl^- with OH^- (40). Although the hydroxide may exist as an intermediate, hemin's reaction is more complicated and results in an oxy-bridged dimer $[PpIX(Fe)]_2O$. However, in the complex, we only observed a single hematin molecule in each TSPO monomer, possibly coordinating an oxygen molecule and a water molecule. Hematin is structurally very similar to hemin and the substrate, PpIX. The only difference is the absence of Fe^{3+} ions within PpIX compared to hemin and hematin.

*Bc*TSPO protein was saturated with hematin and further purified with size exclusion chromatography. The protein complex was concentrated to about 20 mg/mL and mixed with monoolein in a 2:3 (v/v) ratio at room temperature. LCP crystallization conditions were screened using a TTP Mosquito robot with commercial crystallization kits. The successful condition is MemGold MD-1-39 B2: 0.1 M sodium chloride, 0.02 M sodium citrate (pH5.6), 5.5 % (w/v) PEG 3350.

Data Collection, Structure Determination, and Refinement. The diffraction dataset for the *Bc*TSPO/hematin complex was collected at the APS NECA 24-ID-C beamline at 12.66 keV, with 2 s per frame, exposure for 0.3° oscillation frames for 360°. The data were processed with XDS (56). Molecular replacement was performed with Phaser (57) based on apo-state *Bc*TSPO crystal structure (PDB ID: 4RYO) as the search template. The structure was refined with Phenix version 1.16-3549 (58). The structural model was manually built with Coot version 0.9 (59). Data collection and refinement statistics are presented in *SI Appendix*, Tables S1 and S2, respectively.

***Hs*TSPO1 Expression and Purification.** *Hs*TSPO1 (147A) fused with EGFP was constructed with C-terminal Tev-EGFP-10×His-FLAG in the pCEH expression vector. The WT *Hs*TSPO1 (147A) with C-terminal 10xHis tag without ECFP was also constructed in the pCEH expression vector similarly. The plasmids were transfected into Expi293F™ cells following the Expi293F™ expression system user guide. The cell pellets were harvested and stored at −80 °C. *Hs*TSPO1 was purified using the modified protocol as previously published (11). The revised procedures are listed below.

To prepare *Hs*TSPO1 in NCMN particles using NCMNP5-2, we followed a previously published protocol (30). Two protocols were used for the purification of *Hs*TSPO1 using detergents. For protocol 1: Cell membrane fractions of *Hs*TSPO1 were solubilized in buffer A with 1% N-dodecyl-β-D-maltopyranoside (DDM, Anatrace, Inc.) and 0.2% CHS and then passed through the His-Trap HP column. All the following purification buffers contain 0.1% LMNG and 0.02% CHS. For protocol 2: the only difference is the absence of CHS in all the purification buffers. The purity of *Hs*TSPO1 was checked with SDS-PAGE analysis (*SI Appendix*, Fig. S2*A*). Both WT *Hs*TSPO1 without EGFP fusion and *Hs*TSPO1 fused with C-terminal EGFP have similar enzyme activity (*SI Appendix*, Figs. S2 *B* and *C*).

We found here that WT *Hs*TSPO1 is also unstable in many detergents, even in the very mild LMNG; the purification profiles in *SI Appendix*, Fig. S2 *D–F* show the majority of the *Hs*TSPO1 eluted in the void volume fractions, indicating instability of *Hs*TSPO1. This is also consistent with our findings that extended storage of *Hs*TSPO1 is accompanied by the loss of its enzyme activity. Because of the instability of WT *Hs*TSPO1, and the long time to do Tev enzyme cleavage, the purified *Hs*TSPO1 with EGFP fusion (which for convenience we label as *Hs*TSPO1) was used for the photoactivated fluorescence assay of enzyme activity and the intrinsic fluorescence assay of conformation.

Lipidomic Analysis. Lipidomic analysis was done through a fee-based service at the Virginia Commonwealth University Lipidomics/Metabolomics Core.

Synthesis and Characterization of Protoporphyrin IX-2 (PpIX-2). Protoporphyrin IX (PPIX, >95%) was obtained from Sigma-Aldrich. N-(3-Dimethylaminopropyl)-N-ethylcarbodiimide hydrochloride (EDC.HCl, > 98%), dimethyl sulfoxide (DMSO, >99.7%, extra dry over molecular sieve), deuterium dimethyl sulfoxide (DMSO-d6, >99.5% atom D), and dimethylphenylphosphine (DMPP, 97%) were brought from Acros Organics. Cysteamine (Cys, >95%) and 2-methacryloyloxyethyl phosphorychroline (PC, >96%) were purchased from TCI America.

Synthesis of 1 (*SI Appendix*, Figs. S14 and S15). Compound 1 was prepared via a "click" coupling reaction between cysteamine and 2-methacryloyloxyethyl phosphorylcholine, following the previous protocol (60). Briefly, cysteamine (0.37 g, 4.75 mmol, 1 equiv.), 2-methacryloyloxyethyl phosphorylcholine (1.4 g, 4.74 mmol, ~1 equiv.), and DMPP (33.15 mg, 0.24 mmol, 0.05 equiv.) were mixed with 4 ml of DMSO. The mixture was purged with N2 and stirred for 2 d at room temperature before the product was precipitated twice with a mixture of acetone/diethyl ether (2/1 v/v). The residue solvents were removed under a vacuum, giving a pale yellow solid (1.43 g, 81%). 1H NMR (300 MHz, DMSO-d6) δ (ppm) 4.14 to 4.04 (4H, m), 3.81 (2H, t), 3.55 (2H, t), 3.12 (9H, m), 2.80 to 2.53 (6H, m), 1.90 (1H, m), 1.15 (3H, d).

Synthesis of 2 (*SI Appendix*, Figs. S14 and S15). To the mixture of N-(3-dimethyl aminopropyl)-N′-ethyl carbodiimide hydrochloride (38.5 mg, 0.201 mmol, 2.01 equiv.) and 1 (74.4 mg, 0.2 mmol, 2 equiv.) were added protoporphyrin IX (56.3 mg, 0.1 mmol COOH, 1 equiv.) in DMSO (5 mL). The reaction medium was stirred at ambient temperature for 24 h. The crude product was purified using diethyl ether to precipitate and give a dark red solid (1.17 g, 89 %). 1H NMR (300 MHz, DMSO-d6) δ (ppm) 10.31 to 10.15 (4H, m), 8.54 to 8.46 (2H, m), 6.48 to 6.44 (2H, d), 6.25 to 6.22 (2H, d), 6.09 (1H, t), 6.01 (1H, t), 4.40 to 4.31 (4H, m), 4.11 to 4.03 (4H, m), 3.95 to 3.52 (16H, m), 3.16 to 2.62 (44H, m), 1.92 to 1.80 (2H, m), 1.15 to 1.05 (6H, m).

Enzyme Activity Assay. PpIX has special photochemical properties. It features a main Soret band and four Q bands in its UV-Vis scan, and when excited with UV light near 405 nm, it has fluorescence peaks at around 632 nm. Photon oxidation led to a decrease in the intensity of the 632 nm peak and the appearance and increase of a peak at 673 nm (11). Enzyme assays were performed based on the unique photochemical properties of PpIX using a protocol previously published with slight modification (11). Briefly, PpIX is a photosensitive molecule; when it is excited by UV light, especially at around 405 nm, it can absorb photons, reaching an excited state, which can activate triplet-state oxygen molecules into their excited singlet state through energy transfer (this is the major pathway) or superoxide through electron transfer. In the enzyme reaction system, 30 μL of *Bc*TSPO or *Hs*TSPO (1 mg/mL) was separately added into a 230 μL reaction

system with 1 μL saturated PpIX in DMSO. The molar ratio of Hemin, PK11195, or diazepam to TSPO was 100:1. The reaction was performed at room temperature with a Shimadzu RF-5301 PC Spectrofluorophotometer with excitation wavelength at 405 nm, and the fluorescence emission spectrum was recorded between 600 nm and 750 nm.

Analysis of Intrinsic Tryptophan Fluorescence. Intrinsic tryptophan fluorescence analysis of *Hs*TSPO1 in the presence of CHS or absence of CHS and the fluorescence quenching by various ligands of *Hs*TSPO1 or fluorescence shift by various protein denaturing chemicals were performed using the Shimadzu RF-5301P spectrofluorophotometer. The instrumental settings were as follows: EX Wavelength, 295.0 nm; EM Wavelength, Start 300.0 nm; EM Wavelength End, 500.0 nm; Data Interval, 1.0 nm; EX Bandwidth, 1.5 nm; EM Bandwidth 3.0 nm; Sensitivity, High; Response, 0.02 s.

Because of the protein stability issue, as for enzyme activity assays, we also used *Hs*TSPO1 fused to EGFP for these intrinsic fluorescence experiments. EGFP is fused to the TSPO protein through a flexible linker; thus, the water-soluble EGFP domain is unlikely to perturb the tryptophan residues of the TSPO. Moreover, the single tryptophan residue of EGFP (W57) emanates from the central helix and is encased within the β-barrel, thus, where it is highly unlikely to interact with CHS or other hydrophobic ligands specific to *Hs*TSPO1. Therefore, EGFP should have a negligible effect on the analyses of intrinsic tryptophan fluorescence of *Hs*TSPO1, which contains 12 tryptophans.

The protein concentration was experimentally optimized to 1 mg/mL to get a proper fluorescence peak for all the fluorescence analyses. The ligand and denaturing chemical concentrations were experimentally determined, optimized, and detailed in the corresponding figure legends. It is worth noting that PpIX, Hemin, PK11195, and Diazepam are extremely hydrophobic chemicals; accurate concentrations of these chemicals in the experimental aqueous system are challenging to measure. Therefore, instead of giving concentrations of the chemicals, we detailed the procedures of how we set up the experiments so anyone can repeat our experiments.

UPLC–Mass Spectrometric Analysis of Bilindigin and Related PpIX Compounds. Waters Acquity H-Class UPLC was connected to a PDA detector, and an Acquity TQD detector was used for the UPLC–MS analysis of bilindigin and related PpIX compounds. The column used was an Acquity UPLC BEH C18 1.7 μm, 2.1 × 50 mm, with a Vanguard precolumn attached. Solvent A consisted of 90:10 water: acetonitrile with 0.02% formic acid, while solvent B consisted of 90:10 acetonitrile: water with 0.02% formic acid. A gradient run was performed such that solvent B was increased from 0% B to 100% B from 0 to 4 min, followed by a 3 min wash at 100% B and then a return and re-equilibration at 100% A in the next 3 min. The flow rate was maintained at 0.5 mL/min throughout the run. 10 μL of the sample was injected per run. The eluent of the column was connected to a PDA UV detector, which scanned from 254 to 500 nm (limit of the detector), and a 2D channel of 495 nm was chosen to study the compounds. The eluent was then introduced into the TQD detector. The TQD detector was set at positive ionization mode with a capillary voltage of 3.20 kV, a cone voltage of 20 V, an extractor voltage of 1 V, and an RF lens voltage of 0.1 V. The source temperature was set at 150 °C, the desolvation temperature was set at 350 °C, and the desolvation and cone gas flows were set at 750 and 50 L/h, respectively. Scans were made from 200 to 1,990 m/z with a scan duration of 1 s to obtain mass spectra at different time points. For MS–MS analysis, daughter scans were performed using selected parent ion m/z. The source conditions were kept similar to those above. The TQD was set to MS–MS mode, with Argon collision gas flow set at 0.5 mL/min. The collision energy was set at 30, 60, or 90 V to give sequential fragmentation patterns to identify smaller fragments for finer structural details.

Building Human TSPO1 Molecular Model. The model of the *Hs*TSPO1 was built based on the crystal structure of *Bc*TSPO (PDB ID: 4RYO). The MODELLER program was used to generate sets of initial homology models (61). The best model was selected based on the lowest Discrete optimized protein energy score and the highest GA341 assessment score. The stereochemical integrity of the model and its quality were evaluated using PROCHECK to ensure that angles and torsions were within acceptable tolerance limits based on the Ramachandran plot. Model refinement was performed with SYBYL X 2.1.1 (Tripos, LLC). Hydrogens were added to the structures, and atomic charges were set with Gasteiger-Hückel (62), followed by energy minimization to a termination gradient of 0.05 kcal/ (mol Å) or 10,000 iterations.

Docking and Molecular Dynamic Simulation Analysis. GOLD (Genetic Optimization for Ligand Docking) version 5.6 (CCDC, Cambridge, UK) (63) was used to dock the heme, PpIX, PK11195, and diazepam ligands in the putative binding sites in both the human TSPO model and our bacterial homolog. These small molecules were built, and energy was minimized with SYBYL X 2.1.1. All atom types, bond types, and valences were checked with GOLD for optimal compatibility. Binding sites were defined based on the above results and the literature (11). GOLD generated 100 binding pose solutions for the ligand to improve the odds that the optimal pose is explored among the pool calculated by the docking program. Other settings, such as genetic algorithm parameters, no early termination, and no constraints, were used as default. The HINT free energy scoring function developed in Kellogg Lab was used for analyzing the different conformations (64). The hydropathic energy was calculated via HINT within the complex cavities. All HINT parameters and settings were described previously. A cholesterol molecule was docked on the conserved surface region between transmembrane helix 2 and helix 5 (*SI Appendix*, Figs. S10 and S11).

Data, Materials, and Software Availability. Crystallographic data have been deposited in Protein Data Bank (PDB ID: 8VGU) (65).

ACKNOWLEDGMENTS. The Guo laboratory is supported by the Virginia Commonwealth University (VCU) School of Pharmacy and Department of Medicinal Chemistry through startup funds and by the Institute for Structural Biology, Drug Discovery and Development, through laboratory space and facilities. This research was also supported by NIH R01-GM132329 (to Y.G.), NIH R01-GM107462, and P41-GM116799 (W.A.H.). We thank all team members working at NE-CAT beamlines 24-ID-C, and E in the Advanced Photon Source (APS) at Argonne National Laboratory, who helped us collect the crystal dataset. The use of the APS, an Office of Science User Facility operated by the US Department of Energy (DOE) Office of Science by Argonne National Laboratory, was supported by the US DOE under Contract No. DE-AC02-06CH11357. We also thank Rachael Flammia, an undergraduate student in the Department of Chemistry, VCU, for enzyme activity data collection of tryptophan-rich sensory proteins (TSPO). The lipidomic analysis was done by the VCU Lipidomics/Metabolomics Core, which is supported by the NIH-NCI Cancer Center Support Grant P30 CA016059 to the VCU Massey Cancer Center, as well as a shared resource grant (S10RR031535) from the NIH.

Author affiliations: [a]Department of Medicinal Chemistry, Virginia Commonwealth University, Richmond, VA 23298-0540; [b]Institute for Structural Biology, Drug Discovery and Development, Virginia Commonwealth University, Richmond, VA 23298-0133; [c]Department of Biochemistry and Molecular Biophysics, Columbia University, New York, NY 10032; [d]Department of Physiology and Cellular Biophysics, Columbia University, New York, NY 10032; and [e]New York Structural Biology Center, New York, NY 10027

1. C. Braestrup, R. F. Squires, Specific benzodiazepine receptors in rat brain characterized by high affinity [^{3}H] diazepam binding. *Proc. Natl. Acad. Sci. U.S.A.* **74**, 3805–3809 (1977).
2. V. Papadopoulos *et al.*, Translocator protein (18kDa): New nomenclature for the peripheral-type benzodiazepine receptor based on its structure and molecular function. *Trends Pharmacol. Sci.* **27**, 402–409 (2006).
3. L. N. Tu *et al.*, Peripheral benzodiazepine receptor/translocator protein global knock-out mice are viable with no effects on steroid hormone biosynthesis. *J. Biol. Chem.* **289**, 27444–27454 (2014).
4. H. Wang *et al.*, Global deletion of TSPO does not affect the viability and gene expression profile. *PLoS ONE* **11**, e0167307 (2016).
5. C. Hiser, B. L. Montgomery, S. Ferguson-Miller, TSPO protein binding partners in bacteria, animals, and plants. *J. Bioenerg. Biomembr.* **53**, 463–487 (2021).
6. R. Rupprecht *et al.*, Translocator protein (18 kDa) (TSPO) as a therapeutic target for neurological and psychiatric disorders. *Nat. Rev. Drug Discov.* **9**, 971–988 (2010).
7. C. J. Austin, J. Kahlert, M. Kassiou, L. M. Rendina, The translocator protein (TSPO): A novel target for cancer chemotherapy. *Int. J. Biochem. Cell Biol.* **45**, 1212–1216 (2013).
8. J. Musman *et al.*, TSPO ligand prevents mitochondrial sterol accumulation and dysfunction during myocardial ischemia-reperfusion in hypercholesterolemic rats. *Biochem. Pharmacol.* **142**, 87–95 (2017).
9. P. N. Thai *et al.*, Cardiac-specific conditional knockout of the 18-kDa mitochondrial translocator protein protects from pressure overload induced heart failure. *Sci. Rep.* **8**, 16213 (2018).
10. V. Shoshan-Barmatz, S. Pittala, D. Mizrachi, VDAC1 and the TSPO: Expression, interactions, and associated functions in health and disease states. *Int. J. Mol. Sci.* **20**, 3348 (2019).

11. Y. Guo *et al.*, Structure and activity of tryptophan-rich TSPO proteins. *Science* **347**, 551–555 (2015).
12. L. Jaremko, M. Jaremko, K. Giller, S. Becker, M. Zweckstetter, Structure of the mitochondrial translocator protein in complex with a diagnostic ligand. *Science* **343**, 1363–1366 (2014).
13. F. Li, J. Liu, Y. Zheng, R. M. Garavito, S. Ferguson-Miller, Protein structure. Crystal structures of translocator protein (TSPO) and mutant mimic of a human polymorphism. *Science* **347**, 555–558 (2015).
14. F. Bonsack, S. Sukumari-Ramesh, TSPO: An evolutionarily conserved protein with elusive functions. *Int. J. Mo.l Sci.* **19**, 1694 (2018).
15. C. Betlazar, R. J. Middleton, R. Banati, G. J. Liu, The translocator protein (TSPO) in mitochondrial bioenergetics and immune processes. *Cells* **9**, 512 (2020).
16. J. J. Lacapere, L. Duma, S. Finet, M. Kassiou, V. Papadopoulos, Insight into the structural features of TSPO: Implications for drug development. *Trends Pharmacol. Sci.* **41**, 110–122 (2020).
17. Y. Lee, Y. Park, H. Nam, J. W. Lee, S. W. Yu, Translocator protein (TSPO): The new story of the old protein in neuroinflammation. *BMB Rep.* **53**, 20–27 (2020).
18. K. Morohaku *et al.*, Translocator protein/peripheral benzodiazepine receptor is not required for steroid hormone biosynthesis. *Endocrinology* **155**, 89–97 (2014).
19. R. B. Banati *et al.*, Positron emission tomography and functional characterization of a complete PBR/TSPO knockout. *Nat. Commun.* **5**, 5452 (2014).
20. V. Selvaraj, L. N. Tu, D. M. Stocco, Crucial role reported for TSPO in viability and steroidogenesis is a misconception commentary: Conditional steroidogenic cell-targeted deletion of TSPO unveils a crucial role in viability and hormone-dependent steroid formation. *Front. Endocrinol.***7**, 91 (2016).
21. N. Denora, G. Natile, An updated view of translocator protein (TSPO). *Int. J. Mol. Sci.* **18**, 2640 (2017).
22. J. Fan, E. Campioli, C. Sottas, B. Zirkin, V. Papadopoulos, Amhr2-Cre–mediated global TSPO knockout. *J. Endocr. Soc.* **4**, bvaa001 (2020).
23. C. E. Wiers *et al.*, TSPO polymorphism in individuals with alcohol use disorder: Association with cholesterol levels and withdrawal severity. *Addict. Biol.* **26**, e12838 (2021).
24. F. Farhan *et al.*, Deletion of TSPO causes dysregulation of cholesterol metabolism in mouse retina. *Cells* **10**, 3066 (2021).
25. E. Angeloni *et al.*, The human microglial surveillant phenotype is preserved by de novo neurosteroidogenesis through the control of cholesterol homeostasis: Crucial role of 18 kDa translocator protein. *Biochim. Biophys. Acta. Mol. Basis Dis.* **1869**, 166751 (2023).
26. W. Tang *et al.*, Multiplex immunohistochemistry defines two cholesterol metabolism patterns predicting immunotherapeutic outcomes in gastric cancer. *J. Transl. Med.* **21**, 887 (2023).
27. C. Milite *et al.*, Exploiting the 4-phenylquinazoline scaffold for the development of high affinity fluorescent probes for the translocator protein (TSPO). *J. Med. Chem.* **60**, 7897–7909 (2017).
28. V. M. Milenkovic *et al.*, Effects of genetic variants in the TSPO gene on protein structure and stability. *PLoS ONE* **13**, e0195627 (2018).
29. W. Qiu *et al.*, Structure and activity of lipid bilayer within a membrane-protein transporter. *Proc. Natl. Acad. Sci. U.S.A.* **115**, 12985–12990 (2018).
30. K. G. Kroeck, W. Qiu, C. Catalano, T. K. H. Trinh, Y. Guo, Native cell membrane nanoparticles system for membrane protein–protein interaction analysis. *J. Vis. Exp.* **161**, e61298 (2020), https://doi.org/10.3791/61298.
31. L. Yang *et al.*, A native cell membrane nanoparticles system allows for high-quality functional proteoliposome reconstitution. *BBA Adv.* **1**, 100011 (2021).
32. Y. Guo, Detergent-free systems for structural studies of membrane proteins. *Biochem. Soc. Trans.* **49**, 1361–1374 (2021).
33. T. K. H. Trinh, C. Catalano, Y. Guo, Fabrication of membrane proteins in the form of native cell membrane nanoparticles using novel membrane active polymers. *Nanoscale Adv.* **5**, 5932–5940 (2023).
34. C. Ginter, I. Kiburu, O. Boudker, Chemical catalysis by the translocator protein (18 kDa). *Biochemistry* **52**, 3609–11 (2013).
35. J. Dalton, C. A. McAuliffe, D. H. Slater, Reaction between molecular oxygen and photo-excited protoporphyrin IX. *Nature* **235**, 388 (1972).
36. S. Jockusch, C. Bonda, S. Hu, Photostabilization of endogenous porphyrins: Excited state quenching by fused ring cyanoacrylates. *Photochem. Photobiol. Sci.* **13**, 1180–1184 (2014).
37. G. Jaipuria *et al.*, Cholesterol-mediated allosteric regulation of the mitochondrial translocator protein structure. *Nat. Communi.* **8**, 14893 (2017).
38. E. Georges, C. Sottas, Y. Li, V. Papadopoulos, Direct and specific binding of cholesterol to the mitochondrial translocator protein (TSPO) using PhotoClick cholesterol analogue. *J. Biochem.* **170**, 239–243 (2021).
39. T. K. H. Trinh, W. Qiu, M. Thornton, E. E. Carpenter, Y. Guo, A property fine-tuned sulfobetaine cholesterol derivative for membrane protein structural biology. *Biochim. Biophys. Acta. Gen. Subj.* **1865**, 129908 (2021).
40. J. Bauer, J. Fornnarina, High-performance liquid chromatographic analysis of "available" hemin in hematin solutions. *J. Chromatogr.* **283**, 378–382 (1984).
41. C. A. Royer, Probing protein folding and conformational transitions with fluorescence. *Chem. Rev.* **106**, 1769–1784 (2006).
42. W. Wang, Q. Liu, Q. Liu, W. A. Hendrickson, Conformational equilibria in allosteric control of Hsp70 chaperones. *Mol. Cell* **81**, 3919–3933.e7 (2021).
43. R. Qi *et al.*, Allosteric opening of the polypeptide-binding site when an Hsp70 binds ATP. *Nat. Struct. Mol. Biol.* **20**, 900–907 (2013).
44. C. Chipot *et al.*, Perturbations of native membrane protein structure in alkyl phosphocholine detergents: A critical assessment of NMR and biophysical studies. *Chem. Rev.* **118**, 3559–3607 (2018).
45. J. Liu *et al.*, New TSPO crystal structures of mutant and heme-bound forms with altered flexibility, ligand binding, and porphyrin degradation activity. *Biochemistry* **62**, 1262–1273 (2023).
46. F. Li, Y. Xia, J. Meiler, S. Ferguson-Miller, Characterization and modeling of the oligomeric state and ligand binding behavior of purified translocator protein 18 kDa from *Rhodobacter sphaeroides*. *Biochemistry* **52**, 5884–5899 (2013).
47. A. W. Busch, Z. WareJoncas, B. L. Montgomery, Tryptophan-rich sensory protein/translocator protein (TSPO) from cyanobacterium fremyella diplosiphon binds a broad range of functionally relevant tetrapyrroles. *Biochemistry* **56**, 73–84 (2017).
48. F. Li, J. Liu, L. Valls, C. Hiser, S. Ferguson-Miller, Identification of a key cholesterol binding enhancement motif in translocator protein 18 kDa. *Biochemistry* **54**, 1441–1443 (2015).
49. S. G. Andersson, O. Karlberg, B. Canback, C. G. Kurland, On the origin of mitochondria: A genomics perspective. *Philos. Trans. R. Soc. Lond. B. Biol. Sci.* **358**, 165–179 (2003).
50. E. Nji, Y. Chatzikyriakidou, M. Landreh, D. Drew, An engineered thermal-shift screen reveals specific lipid preferences of eukaryotic and prokaryotic membrane proteins. *Nat. Commun.* **9**, 4253 (2018).
51. L. Best, C. Ghadery, N. Pavese, Y. F. Tai, A. P. Strafella, New and old TSPO PET radioligands for imaging brain microglial activation in neurodegenerative disease. *Curr. Neurol. Neurosci. Rep.* **19**, 24 (2019).
52. E. L. Werry *et al.*, Recent developments in TSPO PET imaging as a biomarker of neuroinflammation in neurodegenerative disorders. *Int. J. Mol. Sci.* **20**, 3161 (2019).
53. B. Janssen, R. H. Mach, Development of brain PET imaging agents: Strategies for imaging neuroinflammation in Alzheimer's disease. *Prog. Mol. Biol. Transl. Sci.* **165**, 371–399 (2019).
54. M. Kircher, C. Lapa, Infection and inflammation imaging: Beyond FDG. *PET Clin.* **15**, 215–229 (2020).
55. C. Cavaliere *et al.*, Gliosis and neurodegenerative diseases: The role of PET and MR imaging. *Front. Cell Neurosci.* **14**, 75 (2020).
56. W. Kabsch, XDS. *Acta Crystallogr. D. Biol. Crystallogr.* **66**, 125–132 (2010).
57. A. J. McCoy *et al.*, Phaser crystallographic software. *J. Appl. Cryst.* **40**, 658–674 (2007).
58. P. D. Adams *et al.*, PHENIX: A comprehensive python-based system for macromolecular structure solution. *Acta. Crystallogr. D Biol. Crystallogr.* **66**, 213–221 (2010).
59. P. Emsley, K. Cowtan, Coot: Model-building tools for molecular graphics. *Acta. Crystallogr. D Biol. Crystallogr.* **60**, 2126–2132 (2004).
60. M. C. Fiori, Y. Jiang, G. A. Altenberg, H. Liang, Polymer-encased nanodiscs with improved buffer compatibility. *Sci. Rep.* **7**, 7432 (2017).
61. B. Webb, A. Sali, Comparative protein structure modeling using modeller. *Curr. Protoc. Bioinf.* **54**, 5.6.1–5.6.37 (2016).
62. J. Gasteiger, M. Marsili, Iterative partial equalization of orbital electronegativity–A rapid access to atomic charges. *Tetrahedron* **36**, 3219–3228 (1980).
63. G. Jones, P. Willett, R. C. Glen, A. R. Leach, R. Taylor, Development and validation of a genetic algorithm for flexible docking. *J. Mol. Biol.* **267**, 727–748 (1997).
64. A. Sarkar, G. E. Kellogg, Hydrophobicity–shake flasks, protein folding and drug discovery. *Curr. Top. Med. Chem.* **10**, 67–83 (2010).
65. W. Qiu, Y. Guo, W. A. Hendrickson, Data from "Crystal structure of BcTSPO/Hematin complex." PDB. https://doi.org/10.2210/pdb8VGU/pdb. Deposited 28 December 2023.